DOI: 10.1002/((please add manuscript number))
Article type: Communication

Self-regulating iris based on light-actuated liquid crystal elastomer

Hao Zeng, Owies M. Wani, Piotr Wasylczyk, Radosław Kaczmarek, Arri Priimagi**

Dr. H. Zeng, O. M. Wani, Prof. A. Priimagi
Laboratory of Chemistry and Bioengineering, Tampere University of Technology, P.O. Box 541, FI 33101 Tampere, Finland
E-mail: hao.zeng@tut.fi, arri.priimagi@tut.fi

Dr. P. Wasylczyk
Photonic Nanostructure Facility, Institute of Experimental Physics, Faculty of Physics, University of Warsaw, ul. Pasteura 5, 02-093 Warsaw, Poland

Dr. R. Kaczmarek
Department and Clinic of Ophthalmology, Wrocław Medical University, ul. Borowska 213, 50-556 Wrocław, Poland

Keywords: (iris; biomimetic; photoactuation; liquid crystal elastomer; azobenzene)

Abstract. Iris, found in many animal species, is a biological tissue that can change the aperture (pupil) size to regulate light transmission into the eye in response to varying illumination conditions. The self-regulation of the eye lies behind its auto-focusing ability and large dynamic range, rendering it the ultimate "imaging device" and a continuous source of inspiration in science. In optical imaging devices, adjustable apertures play a vital role as they control the light exposure, the depth of field, and optical aberrations of the systems. Tunable irises demonstrated to date require external control through mechanical actuation, and are not capable of autonomous action in response to changing light intensity without control circuitry. A self-regulating artificial iris would offer new opportunities for device automation and stabilization. Here, we report the first iris-like, liquid-crystal elastomer device that can perform automatic shape-adjustment by reacting to the incident light power density. Similar to natural iris, the device closes under increasing light intensity, and upon reaching the minimum

pupil size, reduces the light transmission by a factor of 7. The light-responsive materials design, together with photoalignment-based control over the molecular orientation, provide a new approach to automatic, self-regulating optical systems based on soft smart materials.

Depending on biological species, pupils come in diverse geometries, comprising ellipses, slits, pin-holes, and crescent shapes, helping animals to adapt to the specific requirements of their living environment.[1] In human iris, the sphincter and dilator muscles control the pupil size in order to stabilize the light transmission into the retina.[2] In all cases, a disturbance in the iris functionality leads to severe visual dysfunctions. Just as in human/animal eyes, adjustable apertures are vital in technological applications, particularly in imaging systems and spectrometers. Photographic devices commonly contain a mechanical iris diaphragm consisting of several thin segments that form an adjustable polygonal aperture, which allows controlling the depth of field, optical aberrations, and other parameters that influence the image quality.[3] Spectrometers implement tunable slits to control the resolution and to adjust the overall signal level during data collection.[4] Recently, compact and tunable aperture devices have been made using different actuation mechanisms, *e.g.*, electromagnetic heating,[5] electro-wetting in micro-fluidics[6,7] and piezo-mechanics.[8] All these iris-like devices are passive in the sense that they require external control (*i.e.*, a separate controller apart from the iris) and *ex-situ* light detection schemes. An iris device that can self-adjust the aperture size in response to incident light intensity would provide access to automated optical systems in environments where no controlling circuits can access, *e.g.*, opto-fluidic channels. However, their technical realization remains a grand challenge.

The only way to realize an iris device that senses the light field is to fabricate it from a material that itself is photo-responsive, and devise a configuration that opens/closes in response to decreasing/increasing light levels. As we show, such actuation can be reached in light-responsive liquid-crystal elastomers (LCEs), which are smart materials that can exhibit

large shape deformation upon illumination.[9-11] Light-responsive LCEs comprise a loosely crosslinked network of liquid-crystalline moieties with controlled molecular alignment, whereas the light-active units can be either part of the polymer network[12] or simply doped into it.[13] The elastic network can undergo reversible shape changes in response to photochemical[9] (*e.g.*, *trans-cis* isomerization) or photothermal[14] stimulus. In either case, the benefit of the light-based actuation scheme relies on remote, non-contact energy supply, and the precise spatial and temporal control over light properties. Several LCE-based soft-robotic devices have been reported exploiting these features, such as micro-swimmers,[15,16] walkers,[17,18] and transportation devices.[19] Self-regulating behavior in light-driven LCE film has been demonstrated in simple photomechanical oscillating systems,[20] and recently in an artificial flytrap device capable of autonomous action based on optical feedback.[21]

Herein, we report an LCE iris that can autonomously open and close by responding to the incident light intensity, without any need for external control circuitry. Mimicking the properties of a natural iris (**Figure 1**a,b), the device opens/closes upon decreasing/increasing light levels. To accomplish the first goal, we use LCE-based soft actuator and light-induced bending as the mechanism responsible for the modification of the aperture size. To fulfil the second point, we implement photoalignment-based control over molecular alignment to achieve radial molecular orientation within the LCE film, and fabricate a structure with 12 radially aligned segments (**Figure 1**c,d). We employ anisotropic thermal expansion within the polymerized LCE to maintain the iris in the open state under low-light conditions, while at increased exposures, light-triggered molecular reorientation forces the iris to close and thus to reduce the aperture size. To the best of our knowledge, this is the first demonstration of artificial iris that is both powered and controlled with light, performing transmission adjustment relying directly on external light intensity.

Bending of a thin strip is the most common way to characterize liquid-crystal polymer actuation under external stimuli.[22-25] From the technological point of view, it is often most

convenient to fabricate an LCE film in a glass cell, with thickness d ranging from a few to a few tens of μm and length l of several millimetres. In such films, bending upon light absorption is due to the strain difference $\Delta\varepsilon$ occurring between the two surfaces, with a simple relationship between the bending angle α and the geometry: $\alpha \approx \Delta\varepsilon \cdot l/d$ ($l >> d$). Such bending film can be extremely sensitive: for d = 10 μm and l = 5 mm, $\Delta\varepsilon$ as low as 0.16% may be sufficient to induce a bending of 90°. Due to this high sensitivity, changes in the bending angle are affected by many parameters such as environmental variations, inhomogeneities in the material composition, or imperfections in the film fabrication process. It is widely accepted that the initial bending existing even when the film is not exposed to light, is due to residual stress in the LC network generated during photopolymerization.[26,27] The nature of the residual stress is complex, depending delicately on the molecular system used. Apart from uniform shrinkage,[28] other reasons for building up the residual stress during polymerization could be for instance opposite diffusion of monoacrylate and diacrylate monomers during photopolymerization,[29] and *cis*-to-*trans* isomerization in the darkness after photopolymerization.[26] However, the initial bending phenomenon has rarely been connected with anisotropic thermal expansion,[30,31] and to the best of our knowledge, it has not been previously utilized in soft actuator design.

Liquid crystal elastomers are anisotropic materials, exhibiting not only optical birefringence but also anisotropic thermal expansion governed by molecular orientation.[23,32] This is pertinent when the photopolymerization is performed at elevated temperatures in order to stabilize the LC phase. **Figure** 2a illustrates an LCE film polymerized at temperature T_p, which is higher than the room temperature T_R. When a strip is cut out from the film, it remains flat only when the environmental temperature T_e is equal to T_p. After polymerization, however, the actuation experiments are typically carried out at room temperature (in our case T_R = 22 °C), tens of °C below the T_p. In a splay-aligned film, different thermal expansion at different film surfaces will create the stress and thus induce spontaneous bending of the film.

When the same film is polymerized at T_R ($T_p = T_R$), no stress is preserved inside the material at T_R and no spontaneous bending occurs. However, when T_e is elevated, the strip bends to the opposite direction, as illustrated in **Figure** 2b. To demonstrate the utility of the anisotropic thermal expansion, we prepared a series of 20 μm thick splay-aligned LCE strips, polymerized them at different temperatures, and monitored the bending angles α (upon no light irradiation) at different temperatures. As shown in **Figure** 2c, an LCE strip polymerized at 40 °C (solid pink dot), shows gradually increasing bending deformation upon slow cooling, reaching the maximum bending at T_R. A strip polymerized at 20 °C (red dots) remains flat at T_R. In **Figure** 2d we plot the α *vs*. temperature difference ΔT between polymerization and room temperature, showing that for $\Delta T > 0$, *i.e.*, when the polymerization temperature is higher than the operation temperature, maximum initial bending occurs when the polymerization temperature is 20-30 °C higher than the operation temperature. With the photopolymerizable mixture we employed, further increase in the polymerization temperature to 60 °C (ΔT = 38 °C) brings the mixture close to the LC-to-isotropic phase transition temperature, T_c = 64 °C, in which case even slight absorption from the polymerizing light can trigger partial phase transition, reduce the order parameter, and thus decrease the bending angle of the LCE strip at T_R. We note that this initial bending (for $\Delta T > 0$) is in the direction opposite to the light-induced bending. Therefore, we can make use of it in our artificial iris design (**Figure** 1c,d), making it open in the dark, and closed upon light illumination, which is opposite to "conventional", commonly used light-induced bending in LCE films.

To realize the LCE iris, it is imperative that all the bending segments actuate symmetrically towards the same central point, requiring the LCE constituents to be radially aligned. Obtaining such alignment using conventional preparation procedures such as rubbing and mask-exposure[17,33,34] is challenging, hence we used photoalignment technique[35-37] to achieve the desired molecular alignment. The sample preparation procedure is illustrated in **Figure 3**. The LC cell (20 μm thick) was constructed such that at the upper surface the LC

molecules adopted homeotropic alignment, while the bottom surface was coated with an azobenzene-based photoalignment layer (PAAD-72, BEAM Co.), allowing us to define the LC alignment with polarization of the incident light (**Figure** 3b,c). To obtain the radial molecular alignment, we used a radial-polarization converter[38] to transform linearly polarized light into azimuthally polarized, as illustrated in **Figure** 3d. The molecules within the photoalignment layer orient themselves in the direction perpendicular to the polarization of the incident light, hence azimuthal polarization gives rise to radial photoalignment (**Figure** 3c,d) and, consequently, radial alignment of the photopolymerizable LC mixture close to the bottom surface of the cell. To make the mixture responsive to visible light (we wanted to avoid using UV light in order to obtain "human-friendly" action) we doped it with Disperse Red 1 (DR1, 4 mol-%). Upon irradiation with wavelengths in the blue–green region of the spectrum, DR1 is known to undergo continuous *trans-cis-trans* cycling, thereby releasing a significant amount of heat. It is the photothermal heating that we employ in our actuator design. The chemical structures of the compounds used in this work are shown in **Figure** 3e. The polymerization was carried out at 45 °C in order to maximize the initial bending (**Figure** 2). After polymerization, the material has a Young's modulus of 2.5 MPa at room temperature (**Figure S1**), and its glass transition temperature is below room temperature, as confirmed by the differential scanning calorimetry curves shown in **Figure S2**. The cross-polarized optical micrograph of the LCE film, shown in the inset of **Figure** 3f, revealed that the radial molecular alignment was preserved after polymerization. After opening the cell, a disc with 14.0 mm diameter (approximately the size of the human iris) with 12 petal-shape segments was cut out (**Figure** 3f). After releasing the stress by annealing at 50 °C, the device spontaneously "opened up" and adapted a flower-like shape at room temperature, with a central hole of about 10 mm in diameter (**Figure** 3g). In this geometry, each "petal" segment is able to deform in response to the local light intensity, as shown in **Movie 1**, where the LCE segments move in response to a scanned light beam. Upon uniform illumination with 470 nm

LED light, all iris segments bend inwards and the aperture closes (**Figure** 3h, **Movie 2**). For more details on the fabrication process, we direct the reader to the Supporting Information.

To characterize the performance of the device, a 488 nm laser beam with a diameter of 12 mm was projected onto the iris, and the transmitted light as a function of the incident light power was measured (**Figure** 4a). When the incident power was slowly increased from 20 to 120 mW, all segments deformed inwards and gradually reduced the aperture size. For laser powers above 120 mW, some segments closed completely, resulting in a rapid decrease in the iris transmission. At around 180 mW all the segments bent inwards and the aperture closed, reaching transmission as low as 10%. The self-regulating iris is able to adjust the transmitted light power across a 200 mW range: approximately 20 mW of light is transmitted for both 30 mW input (corresponding to 70% transmission) and 200 mW input (10% transmission; red line in **Figure** 4a). **Figure** 4b shows the iris response dynamics after the device is illuminated instantaneously with 270 $mWcm^{-2}$ intensity and the output power through the iris is recorded. The decreasing curve of the output power comprises several steps, each of them corresponding to one or few iris segments closing. Differences in the closure time for different segments are attributed to fabrication defects (e.g. slight variation of thickness and molecular alignment between segments), and high sensitivity of the bending actuation. Images of the iris at different stages of the closing action are shown in the insets of **Figure** 4b, revealing the separated closed segments and asymmetric shape of the aperture at the intermediate stages. The asymmetric shape of the aperture does not harm the image processing in photographic application, but it may offer novel optical functionalities. The diversity in the material design and the versatility of the photoalignment-based patterning technique[39] also provide the opportunities to realize artificial irises with different shapes and photodeformation modes, mimicking the diverse iris geometries observed for different animal species.[1] Real-time closing action is shown in **Movie 3**, where an iris is placed in front of a LED light source and responds to blocking the light beam. **Figure** 4c plots the closure times

for the 12 individual segments under different incident light intensities. Upon low-intensity excitation, the closure time varies significantly for the different segments, whereas the variation is much smaller at high light intensities. The statistical analysis of the closure times is shown in **Figure S3** of the Supporting Information. The complete closure action takes place in 30 s upon 230 mW cm^{-2} incident light intensity, and in less than 5 s upon 300 mW cm^{-2} irradiation.

We attribute the closing action of the iris mostly to photothermal heating of the LCE film.[14] The heating is demonstrated in **Movie 4**, showing the light-induced temperature increase of the LCE film imaged with an infrared camera, revealing that the iris becomes flat (all segments closed) when the maximum temperature within the segments reaches 49 °C. This value is consistent with the polymerization temperature (45 °C), in which case no initial bending due to the anisotropic thermal expansion is expected (see the pink dots in **Figure** 2c). Different from photochemical (isomerization-induced) actuation that is strongly influenced by optical density,[9] the light-induced temperature increase is insensitive to light penetration depth into the material. During photothermal actuation, both material surfaces experience similar temperature increase due to fast heat conduction across the relatively thin film. The temperature-dependent actuation properties allow us to also obtain an iris device with opposite action, i.e., one that is closed in the dark and opens upon light irradiation. This is demonstrated in **Movie 5**, showing an iris deforming on a hot plate at 50 °C, closing up without light and opening again upon illumination. As an additional benefit, the system can be made sensitive to different wavelengths of light, simply by changing the dye inducing the photothermal effect, while sensitivity over broader spectral range can be obtained by doping the system with several dyes or broadband absorbers. We note that the dyes do not have to be azobenzenes,[14] as we believe photoisomerization to play only a minor role in the performance of the iris. However, if photochemical actuation was implemented instead of light-induced heating, the iris functionality could be obtained also in liquid environment,

paving way towards optofluidic applications or actuation in biologically relevant environments.

To conclude, we report what we believe to be the first artificial iris that can self-regulate the aperture size in direct response to the incident light intensity variations. We employ anisotropic thermal expansion of LCEs in order to maintain the iris in the open state in the dark, while radial molecular alignment was used to induce circularly symmetric actuation of the iris segments, thus closing the aperture upon illumination with visible light. The diversity of material design and sophisticated form of actuation paves way towards adjustable soft optics with light-control capacity, and offers alternatives to realize micro-robotic systems with smart features, such as self-recognition, stabilization and automatic manipulation.

Experimental Section

Materials: The LCE actuator is made by polymerization of a mixture that contains 75 mol% of LC monomer 4-Methoxybenzoic acid 4-(6-acryloyloxyhexyloxy)phenyl ester, 20 mol% of LC crosslinker 1,4-Bis-[4-(3-acryloyloxypropyloxy)benzoyloxy]-2-methylbenzene (both purchased from Synthon chemicals), 4 mol% of light-responsive molecule N-Ethyl-N-(2-hydroxyethyl)-4-(4-nitrophenylazo)aniline (Disperse Red 1, Sigma Aldrich), and 1 mol% of photo-initiator (2,2-Dimethoxy-2-phenylacetophenone, Sigma Aldrich). All compounds were used as received. For sample preparation details, see the Supporting Information.

Characterization: Absorption spectra were measured with a custom-modified UV-Vis spectrophotometer (Cary 60 UV-Vis, Agilent Technologies) with a polarization controller. Optical images and movies were recorded by using a Canon 5D Mark III camera (f = 100 mm lens), and thermal images were recorded with an infrared camera (FLIR T420BX, close-up 2×lens, 50 μm resolution). Spatially filtered light from a continuous-wave laser (488 nm, Coherent Genesis CX SLM) was expanded to a diameter of 12 mm and controlled with a

beam shutter before impinging on the soft iris. The light impinged onto the iris always from the side with bent segments, in order to avoid shadowing by the exterior sections of the iris. The power of incident and transmitted light were measured with a microscope-slide power sensor (Thorlabs, S170C). For the iris actuation demonstrations (Movies 1, 2, 3, 5), an LED (Prior Scientific, 470 nm) with tunable output power was used for light actuation. For temperature-dependent bending angle measurements, LCE strips were immersed in a water bath on a heating stage. An infrared camera was used to monitor the water temperature, and the images at different water temperatures were captured using the Canon camera in the top view. No sensitivity to humidity was found in the LCE. For measuring the mechanical properties, a planar-aligned LCE sample with dimensions $10 \times 2 \times 0.05$ mm^3 was cut along the nematic director, and vertically attached to a force sensor and a linear motor stage. The stress–strain curve was measured at room temperature. Differential scanning calorimetry measurement was performed with a Mettler Toledo Star DSC821e instrument, using heating/cooling speeds of 10 °C min^{-1}.

Supporting Information

Supporting Information is available from the Wiley Online Library or from the author.

Acknowledgements

A. P. gratefully acknowledges the financial support of the European Research Council (Starting Grant project PHOTOTUNE; Agreement No. 679646). O. W. is thankful to the graduate school of Tampere University of Technology (TUT), and H. Z. to the TUT postdoctoral fellowship program, for supporting this work. We are indebted to S. L. Oscurato and M. Saccone for assistance with photoalignment patterning and DSC experiments, respectively. We thank Dr. Nelson Tabiryan from BEAM co. (http://www.beamco.com) for providing the photoalignment material PAAD-72 for our use.

Received: ((will be filled in by the editorial staff))
Revised: ((will be filled in by the editorial staff))
Published online: ((will be filled in by the editorial staff))

References

1. J. González-Martín-Moro, F. Gómez-Sanz, A. Sales-Sanz, E. Huguet-Baudin, J. Murube-del-Castillo, *Arch. Soc. Esp. Oftalmol.* **2014**, *89*, 484.

2. R. S. Snell and M. A. Lemp, Movements of the eyeball and the extraocular muscles, in Clinical Anatomy of the Eye, Second Edition, Blackwell Science Ltd., Oxford, UK, 1997.

3. E. Allen and S. Triantaphillidou, The Manual of Photography (10th Edition), Elsevier Ltd, Oxford, UK, 2012.

4. J. M. Lerner, *Cytom. Part A* **2006**, *69A*, 712.

5. S. Schuhladen, F. Preller, R. Rix, S. Petsch, R. Zentel, H. Zappe. *Adv. Mater.* **2014**, *26*, 7247.

6. P. Muller, R. Feuerstein, H. Zappe, *J. Microelectromech. Syst.* **2012**, *21*, 1156.

7. S. Schuhladen, K. Banerjee, M. Sturmer, P. Muller, U. Wallrabe, H. Zappe. *Light Sci. Appl.* **2016**, *5*, e16005.

8. J. Draheim, T. Burger, J. G. Korvink, U. Wallrabe, *Opt. Lett.* **2011**, *36*, 2032.

9. T. Ikeda, J.-i. Mamiya, Y. Yu, *Angew. Chem. Int. Ed.* **2007**, *46*, 506.

10. C. Ohm, M. Brehmer, R. Zentel, *Adv. Mater.* **2010**, *22*, 3366.

11. M. H. Li, P. Keller, B. Li, X. Wang, M. Brunet, *Adv. Mater.* **2003**, *15*, 569.

12. C. L. van Oosten, C. W. M. Bastiaansen, D. J. Broer, *Nat. Mater.* **2009**, *8*, 677.

13. M. Camacho-Lopez, H. Finkelmann, P. Palffy-Muhoray, M. Shelley, *Nat. Mater.* **2004**, *3*, 307.

14. A. H. Gelebart, G. Vantomme, B. E. W. Meijer, D. J. Broer, *Adv. Mater.*, DOI: 10.1002/adma.201606712.

15. C. Huang, J-a. Lv, X. Tian, Y. Wang, Y. Yu, J. Liu. *Sci. Rep.* **2015**, *5*, 17414.

16. S. Palagi, A. G. Mark, S. Y. Reigh, K. Melde, T. Qiu, H. Zeng, C. Parmeggiani, D. Martella, A. Sanchez-Castillo, N. Kapernaum, F. Giesselmann, D. S. Wiersma, E. Lauga, P. Fischer. *Nat. Mater.* **2016**, *15*, 647.

17. M. Rogoz, H. Zeng, C. Xuan, D. S. Wiersma, P. Wasylczyk, *Adv. Opt. Mater.* **2016**, *4*, 1689.

18. H. Zeng, P. Wasylczyk , C. Parmeggiani , D. Martella , M. Burresi, D. S. Wiersma. *Adv. Mater.* **2015**, *27*, 3883.

19. E. Kizilkan, J. Strueben, A. Staubitz, S. N. Gorb, *Sci. Robot.* **2017**, *2*, eaak9454.

20. T. J. White, N. V. Tabiryan, S. V. Serak, U. A. Hrozhyk, V. P. Tondiglia, H. Koerner, R. A. Vaiaa, T. J. Bunning. *Soft Matter* **2008**, *4*, 1796.

21. O. M. Wani, H. Zeng, A. Priimagi, *Nat. Commun.*, in press.

22. S. Iamsaard, S. J. Aßhoff, B. Matt, T. Kudernac, J. J. L. M. Cornelissen, S. P. Fletcher, N. Katsonis, *Nat. Chem.* **2014**, *6*, 229.

23. G. N. Mol, K. D. Harris, C. W. M. Bastiaansen, D. J. Broer, *Adv. Funct. Mater.* **2005**, *15*, 1155.

24. D. Corbett, M. Warner, *Liq. Cryst.* **2009**, *36*, 1263.

25. C. L. van Oosten, D. Corbett, D. Davies, M. Warner, C. W. M. Bastiaansen, D. J. Broer, *Macromolecules* **2008**, *41*, 8592.

26. K. Kumar, C. Knie, D. Bleger, M. A. Peletier, H. Friedrich, S. Hecht, D. J. Broer, M. G. Debije, A. P. H. J. Schenning, *Nat. Commun.* **2016**, *7*, 11975.

27. Y. Sawa, F. Ye, K. Urayama, T. Takigawa, V. Gimenez-Pinto, R. L. B. Selinger, J. V. Selinger, *Proc. Natl. Acad. Sci. USA* **2011**, *108*, 6364.

28. R. M. Carvalho, J. C. Pereira, M. Yoshiyama, D. H. Pashley. *Oper. Dent.* **1996**, *21*, 17.

29. C. F. van Nostrum, R. J. M. Nolte, D. J. Broer, T. Fuhrman, J. H. Wendorff, *Chem. Mater.* **1998**, *10*, 135.

30. L. T. de Haan, V. Gimenez-Pinto, A. Konya, T.-S. Nguyen, J. M. N. Verjans, C. Sánchez-Somolinos, J. V. Selinger, R. L. B. Selinger, D. J. Broer, *Adv. Funct. Mater.* **2014**, *24*, 1251.

31. J. J. Wie, K. M. Lee, T. H. Ware, T. J. White, *Macromolecules* **2015**, *48*, 1087.

32. D. J. Broer, G. N. Mol, *Polym. Eng. Sci.* **1991**, *31*, 625.

33. S. Varghese, S. Narayanankutty, C. W. M. Bastiaansen, G. P. Crawford, D. J. Broer, *Adv. Matt.* **2004**, *16*, 1600.

34. L. T. de Haan, C. Sánchez-Somolinos, C. M. W. Bastiaansen, A. P. H. J. Schenning, D. J. Broer, *Angew. Chem. Int. Ed.* **2012**, *51*, 12469.

35. T. H. Ware, M. E. McConney, J. J. Wie, V. P. Tondiglia, T. J. White, *Science* **2015**, *347*, 982.

36. O. Yaroshchuk, Y. Reznikov, *J. Mater. Chem.* **2011**, *22*, 286.

37. T. Seki, S. Nagano, M. Hara, *Polymer*, **2013**, *54*, 6053.

38. M. Stalder, M. Schadt, *Opt. Lett.* **1996**, *21*, 1948.

39. M. E. McConney, A. Martinez, V. P. Tondiglia, K. M. Lee, D. Langley, I. I. Smalyukh, T. J. White, *Adv. Mater.* **2013**, *25*, 5880.

Figure 1. a, Human iris closes in a bright environment and **b**, opens in the dark. **c,** Schematic drawing of the light-driven iris at its closed state, where light illumination triggers petal segments to bend inwards and to reduce the aperture size. **d**, The iris is open under weak/no light conditions, when the anisotropic thermal expansion induces bending in the segments, thus opening the aperture.

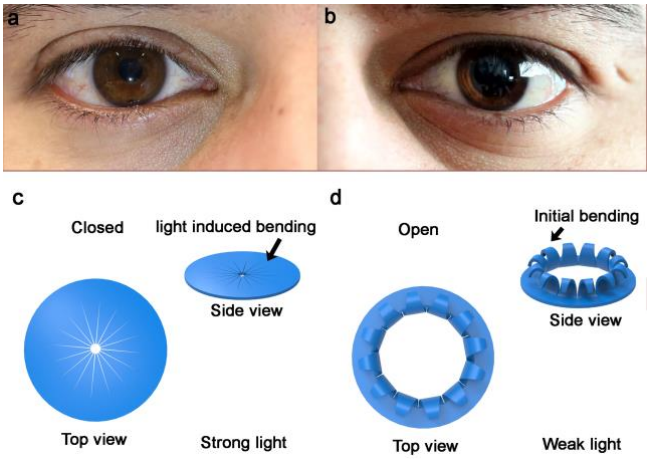

Figure 2. a, Schematic drawing of a splay-bend LCE strip polymerized at an elevated temperature ($T_p > T_R$). It remains flat when the environmental temperature $T_e = T_p$, and spontaneously bends towards the homeotropic direction due to anisotropic thermal expansion when the temperature is reduced to T_R. **b**, The same strip polymerized at T_R, remains flat at T_R and bends to the opposite direction at an elevated temperature ($T_e > T_R$). **c,** The measured bending angle α of LCE strips polymerized at different temperatures T_p. The two LCE strips remain flat at the polymerization temperature ($\alpha = 0$, solid dots on the x-axis), and bend with different angles when environmental temperature is changed (empty circles). Insets: photographs of the LCE strips (6×1×0.02 mm^3) at different temperatures. **d**, Bending angle *vs.* temperature difference ΔT between polymerization temperature and room temperature. Inset: schematic drawing of the anisotropic thermal expansion bending direction with respect to the splayed molecular orientation within the strip. Error bars in **c** and **b** indicate standard deviation for 3 independent measurements.

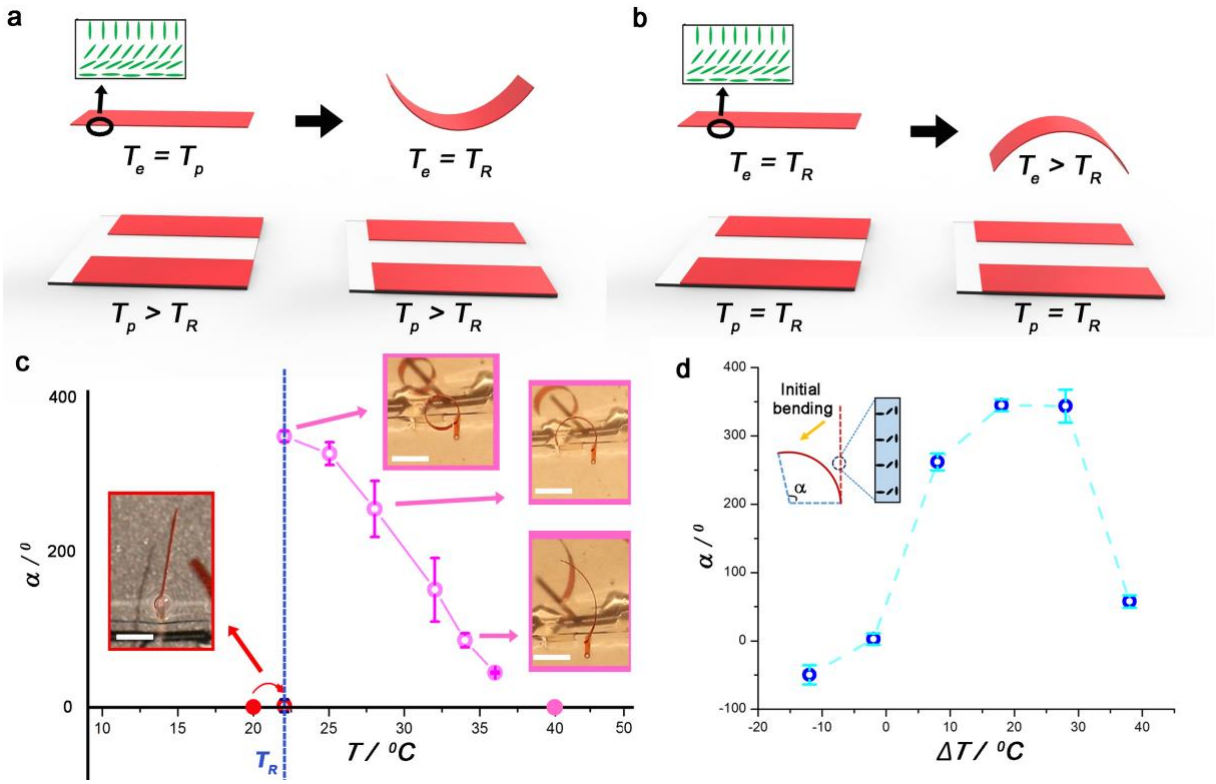

Figure 3. Schematic of the soft iris fabrication process: **a**, A 20 µm cell is prepared by placing together two glass slides, coated with a homeotropic alignment layer on the top and photoalignment layer at the bottom. **b**, LC monomer mixture is infiltrated into the cell and it adapts a centrally-symmetric splayed alignment, directed by **c**, molecular orientation at the top and bottom interfaces. **d**, Schematic of the photoalignment setup. A linearly polarized 488 nm laser beam is converted into azimuthally polarized by using a polarization converter, and then projected onto the substrate coated with the photoalignment layer, due to which the azobenzene molecules within the photoalignment layer adapt radial distribution. **e**, Chemical composition of the LC mixture used. **f**, Optical image of the polymerized LCE film cut out with a circle and with 12 petal-like segments. Inset: cross-polarized image of the film before cutting. **g**. Soft LCE iris in the open state when no light impinges on it. **h**, The iris closes upon light illumination (470 nm, 250 mW cm^{-2}). Scale bars are 5 mm.

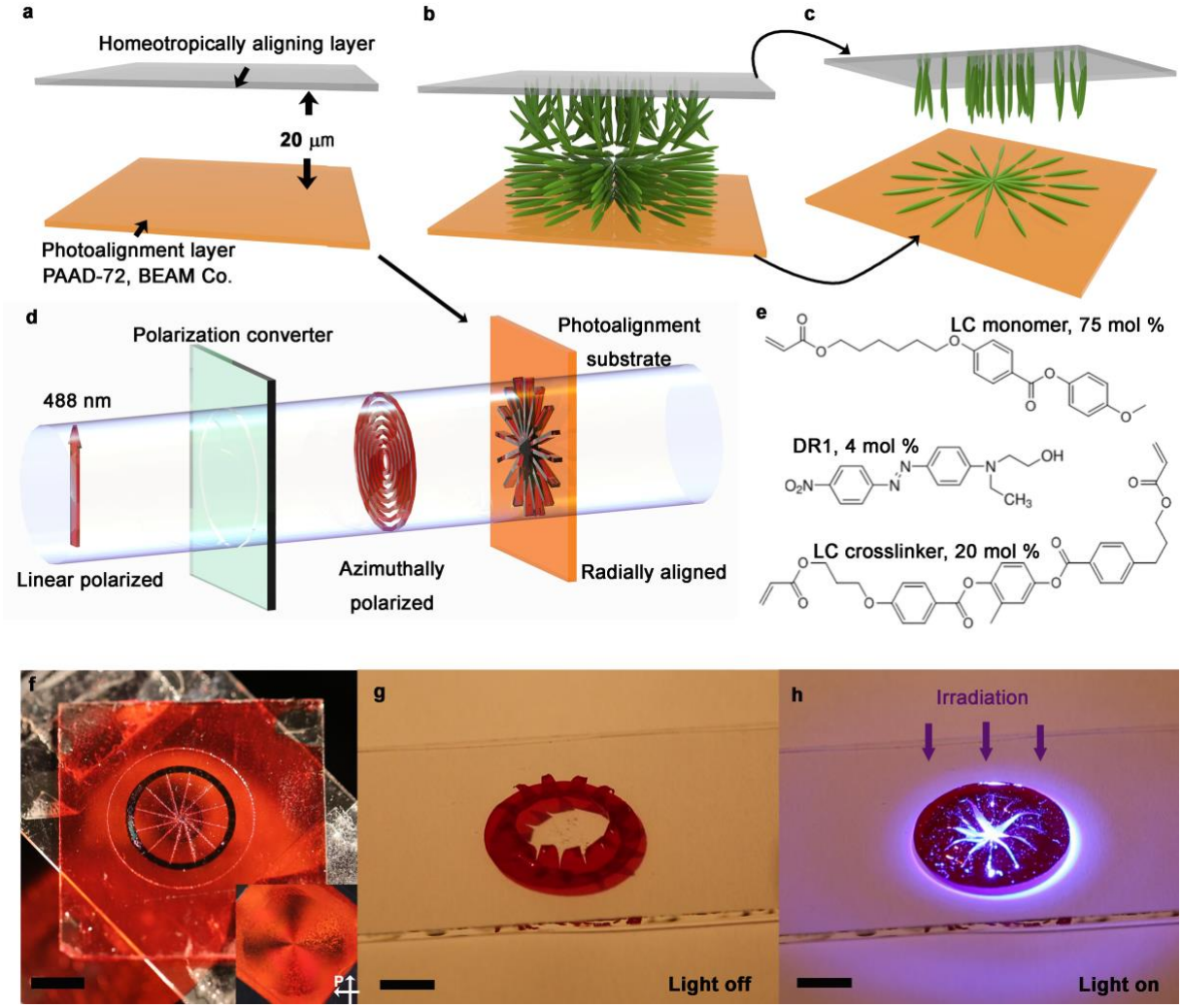

Figure 4. a, Measured transmission (black dots) and transmitted power (red dots) at different input powers. Light source: 488 nm laser with circular polarization; Beam diameter: 12 mm. Error bars indicate standard deviation for 3 independent measurements. Transmitted power presents the average output power from 3 independent measurements, and the dashed line represents the case of 100% transmission through the device. **b**, Measured output power at different times after switching on the light at t = 0 s. Intensity: 270 mW·cm^{-2}. Insets: photographs of the iris at different stages. An optical filter is used to block wavelengths below 500 nm. **c**, Closure time for 12 petal segments at different illumination intensities. The last closed segment defines the complete closure time.

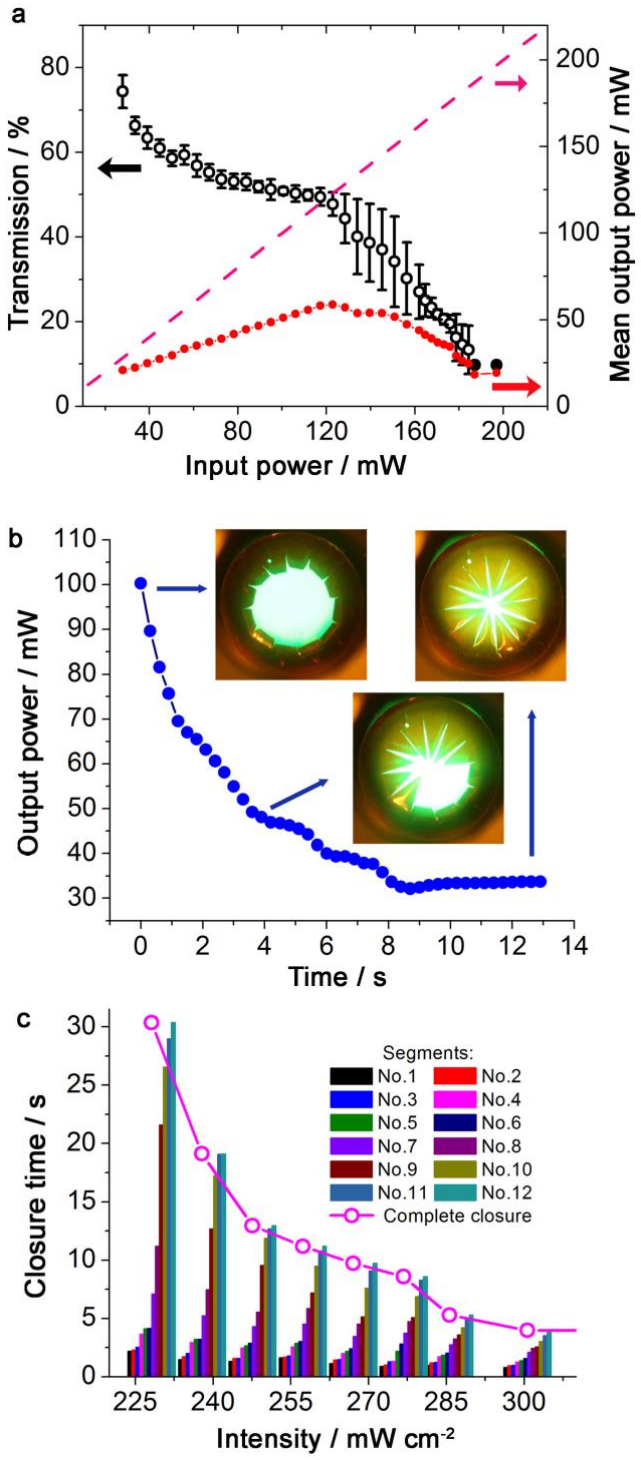

The table of contents:

Iris is a biological tissue that can change the pupil size to stabilize the light transmission into the eye. We report an iris-inspired soft device that can automatically adjust aperture size in response to the change of incident light intensity. The device is made of radially photoaligned liquid crystal elastomer, using anisotropic thermal expansion to realize the desired photoactuation mode.

Keywords: iris; biomimetic; photoactuation; liquid crystal elastomer; azobenzene

Hao Zeng*, Owies M. Wani, Piotr Wasylczyk, Radosław Kaczmarek, Arri Priimagi*

Self-regulating iris based on light-actuable liquid crystal elastomer

ToC figure: